JOURNAL OF COMPUTATIONAL PHYSICS 87, 328–348 (1990)

Coupled Fully Implicit Solution Procedure for the Steady Incompressible Navier–Stokes Equations

F. SOTIROPOULOS AND S. ABDALLAH*

Applied Research Laboratory, The Pennsylvania State University, Post Office Box 30, State College, Pennsylvania 16804

Received June 29, 1988; revised May 10, 1989

This paper presents a new fully implicit procedure for the solution of the steady incompressible Navier–Stokes equations in primitive variables. The momentum equations are coupled with a Poisson-type equation for the pressure and solved using the Beam and Warming approximate factorization method. The present formulation does not require the iterative solution of the pressure equation at each time step. Thus, the major drawback of the pressure-Poisson approach, which made it prohibitively expensive for complex three-dimensional applications, is eliminated. Numerical solutions for the problem of the two-dimensional driven cavity are obtained using a non-staggered grid at $Re = 100$, 400, and 1000. All the computed results are obtained without any artificial dissipation. This feature of the present procedure demonstrates its excellent convergence and stability characteristics. Those characteristics result from the coupling of the pressure equation, which is elliptic in space, with the momentum equations.

INTRODUCTION

Implicit approximate factorization techniques have been developed and successfully applied [1, 2] for time marching solutions of the compressible Navier–Stokes equations. These techniques have desirable stability characteristics and are numerically robust. The absence of the time derivative of the pressure from the incompressible continuity equation, however, prohibits the use of these techniques for the incompressible case.

Chorin [3] modified the incompressible continuity equation by adding a time derivative term for the pressure. Thus the flow becomes artificially compressible, since pressure waves of finite speed are introduced in the incompressible flow field as a medium to distribute the pressure. The resulting system of the governing equations is solved by using approximate factorization techniques developed for compressible flows. The method was applied by Steger and Kutler [4], Kwak *et al.* [5], and Choi and Merkle [6].

Harlow and Welch [7] proposed another approach to solve the incompressible

* Present address: Dept. of Aerospace Eng. and Eng. Mechanics, University of Cincinnati, Cincinnati, OH 45221.

0021-9991/90 $3.00

Navier–Stokes equations. In this approach the continuity equation is replaced by a Poisson equation for the pressure. The system of the governing equations consists, then, of the unsteady momentum equations, which are parabolic in time, and the pressure Poisson equation, which is elliptic in space. This difference in the nature of the governing equations requires the explicit treatment of the pressure and its derivatives in the momentum equations. As proposed by Harlow and Welch, this method was restricted to staggered grids. Recently, the technique was modified so that the pressure equation could be solved on non-staggered grids [8]. Non-staggered grids have advantages over staggered grids, in complex geometries, in non-orthogonal curvilinear coordinates and when using complex numerical techniques such as the multi-grid method. Explicit and semi-implicit pressure Poisson solvers have been developed for the solution of the incompressible Navier–Stokes equations on non-staggered grids. In Ref. [9], the momentum equations are solved by an explicit time marching method, while in Ref. [10] an implicit approach is employed. In both techniques, the pressure in the momentum equations is evaluated explicitly. Therefore, the pressure Poisson equation is solved iteratively at each time step before advancing the solution to the next time level. The iterative solution of the pressure equation at each time step increases considerably the computation time and makes the pressure Poisson solvers prohibitively expensive for complex three dimensional applications [5].

In the present study, the pressure Poisson equation approach is used to develop a new fully implicit method for the solution of the steady incompressible equations on non-staggered grids. An alternative approach for solving the elliptic pressure equation by time marching procedures is considered. A time derivative of the pressure is added to the pressure equation transforming it into a parabolic equation in time, the transient solutions of which have no physical meaning. The time dependent momentum equations and the modified pressure equation are coupled and solved by the Beam and Warming approximate factorization technique in a two-dimensional driven cavity. In this formulation, the pressure terms in the momentum equations are evaluated implicitly and linearized in time in exactly the same way as the velocity terms. In other words, the velocity and pressure fields are simultaneously advanced to the next time level and consequently, no iterative solution of the pressure equation is necessary at each time step. The consistent finite-difference scheme for the pressure equation proposed by Abdallah [8] is used to numerically satisfy the compatibility between the right-hand side of the equation and the Neumann boundary conditions.

The coupling of the pressure equation with the momentum equations results in a very stable and robust numerical scheme. The pressure Poisson equation, which is elliptic in space, introduces into the system of the governing equations dissipative terms which are independent of the Reynolds number (second-order spatial derivatives of the pressure). Thus, stable computations are performed over a wide range of Reynolds numbers without adding any explicit artificial dissipation to the system of the governing equations, even though central differencing is used for the spatial discretization of the convective terms. However, the computed velocity

profiles showed a slight waviness in the inviscid core of the cavity, at high Reynolds numbers. This point is further discussed in the results section. All the computed results are obtained using a non-staggered clustered grid. The convergence histories as well as the results for the pressure, the vorticity and the velocity are presented and compared with other numerical results at Re = 100, 400, and 1000.

Mathematical Formulation

The continuity and momentum equations for incompressible, laminar fluid flow are written in Cartesian coordinates. Although the analysis is performed for two-dimensional flow, it is applicable for three dimensions:

Continuity Equation

$$\frac{\partial u}{\partial x}+\frac{\partial v}{\partial y}=0 \tag{1}$$

x-momentum Equation

$$\frac{\partial u}{\partial t}+u\frac{\partial u}{\partial x}+v\frac{\partial u}{\partial y}=-\frac{\partial P}{\partial x}+\frac{1}{\mathrm{Re}}\left(\frac{\partial^2 u}{\partial x^2}+\frac{\partial^2 u}{\partial y^2}\right) \tag{2}$$

y-momentum Equation

$$\frac{\partial v}{\partial t}+u\frac{\partial v}{\partial x}+v\frac{\partial v}{\partial y}=-\frac{\partial P}{\partial y}+\frac{1}{\mathrm{Re}}\left(\frac{\partial^2 v}{\partial x^2}+\frac{\partial^2 v}{\partial y^2}\right). \tag{3}$$

In the above equations the dependent variables P, u, v are the static pressure divided by the density, velocity component in x-direction, and velocity component in y-direction, respectively. Re is the Reynolds number.

The governing equations (1)–(3) are solved using the primitive variable formulation on non-staggered grids. The momentum equations (2) and (3) are solved for the velocity components u and v by marching in time. The pressure is computed from a Poisson-type equation derived from the divergence of the momentum equation.

Pressure Poisson Equation

By differentiating Eq. (2), w.r.t. x and Eq. (3) w.r.t. y and adding them, we obtain

$$\frac{\partial^2 P}{\partial x^2}+\frac{\partial^2 P}{\partial y^2}=\sigma-\frac{\partial D}{\partial t}, \tag{4}$$

where

$$\sigma=-\frac{\partial}{\partial x}\left(u\frac{\partial u}{\partial x}+v\frac{\partial u}{\partial y}\right)-\frac{\partial}{\partial y}\left(u\frac{\partial v}{\partial x}+v\frac{\partial v}{\partial y}\right) \tag{4a}$$

and

$$D = \frac{\partial u}{\partial x} + \frac{\partial v}{\partial y}. \tag{4b}$$

Equation (4) is a second-order elliptic partial differential equation for the pressure. It is used instead of the continuity equation in the system (1)–(3): To enforce the continuity equation (1), the unsteady term in the pressure equation (4) is approximated as the unsteady terms of the momentum equations and $D(t + \Delta t)$ is set equal to zero. This point will be further discussed in the numerical solution section.

Boundary Conditions for the Pressure Equation

Neumann and Dirchlet boundary conditions for the pressure can be obtained by using the normal-and tangential-momentum equations at the boundaries [11]. The Dirichlet boundary conditions, however, require the additional step of integrating the tangential momentum equation along the boundary contour of the solution domain. It is also shown in Ref. [12] that the iterative solutions of the governing equations (2)–(4) with Neumann boundary conditions, for the pressure equation, converge faster than the Dirichlet case. Thus, the Neumann boundary conditions are used here.

Neumann Boundary Conditions

At an $x =$ constant boundary,

$$\frac{\partial P}{\partial x} = -\left(u\frac{\partial u}{\partial x} + v\frac{\partial u}{\partial y}\right) - \frac{1}{\mathrm{Re}}\frac{\partial \omega}{\partial y}. \tag{5a}$$

At a $y =$ constant boundary,

$$\frac{\partial P}{\partial y} = -\left(u\frac{\partial v}{\partial x} + v\frac{\partial v}{\partial y}\right) + \frac{1}{\mathrm{Re}}\frac{\partial \omega}{\partial x} \tag{5b}$$

$$\omega = \frac{\partial v}{\partial x} - \frac{\partial u}{\partial y}. \tag{5c}$$

Solutions for the pressure Poisson equation (4) with Neumann boundary conditions (5) exist only if a compatibility condition is satisfied.

Compatibility Condition

This condition is derived from Green's theorem or by direct integration of Eq. (4) over the solution domain

$$\iint \left(\sigma - \frac{\partial D}{\partial t}\right) dx\, dy = \oint \frac{\partial P}{\partial n}\, dS, \tag{6}$$

where n is the outward unit vector normal to the boundary contour S which encloses the solution domain.

Failure to satisfy Eq. (6) results in non-convergent iterative solutions for Eq. (4) [13], because a solution does not exist. The compatibility condition (6) is automatically satisfied on staggered grids; however, this is not the case for non-staggered grids. The consistent finite-difference method developed by Abdallah [8], which ensures the satisfaction of the compatibility condition on non-staggered grids, is used for the solution of Eq. (4). The method consists of the following three steps:

(1) Write the Poisson equation in a conservative form.

(2) Write the viscous terms in the momentum equations in terms of the vorticity.

(3) Use consistent finite-difference approximation for the pressure equation and the Neumann boundary conditions.

For more details about the method, the reader is referred to Ref. [8, 9].

Solution Procedure

The governing equations have been solved, so far, with the pressure equation uncoupled from the momentum equations because the momentum equations are parabolic in time and the pressure equation is elliptic in space. In Ref. [9, 14] the momentum equations are solved by explicit time marching techniques. In Ref. [10] the momentum equations are coupled and solved implicitly using the approximate factorization technique of Beam and Warming. In both methods, the pressure Poisson equation is solved at each time step by the successive over-relaxation approach. Therefore, in both methods, the pressure is evaluated at the old time level and consequently the pressure derivatives are moved to the right-hand side of the momentum equations (2) and (3).

Present Method

In the present study, a fully implicit technique is developed for the solution of the momentum equations coupled with the pressure Poisson equation. The main difficulty in coupling Eq. (2)–(4) is the absence of a time derivative term from the pressure equation (4). In order to overcome this difficulty, an alternative procedure for solving elliptic-type equations by time dependent solvers is considered. The addition of a first-order time derivative term for the pressure to Eq. (4) makes it a diffusion-like parabolic equation in time,

$$-\beta \frac{\partial P}{\partial t} + \frac{\partial^2 P}{\partial x^2} + \frac{\partial^2 P}{\partial y^2} = \sigma - \frac{\partial D}{\partial t}, \tag{7}$$

where β is a positive constant to accelerate convergence.

Although, the pressure equation (7) is different from Eq. (4) it has the same

steady state solution. It is important to mention here that the transient solutions of Eq. (7) are not physically meaningful.

The governing equations (2), (3), and (7) are coupled as

$$\Gamma \frac{\partial Q}{\partial t} + \frac{\partial E}{\partial x} + \frac{\partial F}{\partial y} = \frac{\partial}{\partial x}(E_v) + \frac{\partial}{\partial y}(F_v) + H, \tag{8}$$

where

$$\Gamma = \text{diag}(1, 1, \beta) \tag{8a}$$

$$Q = (u, v, P)^{\mathrm{T}} \tag{8b}$$

$$E = (u^2 + P, uv, 0)^{\mathrm{T}} \tag{8c}$$

$$F = (uv, v^2 + P, 0)^{\mathrm{T}} \tag{8d}$$

$$E_v = \left(\frac{1}{\mathrm{Re}}\frac{\partial u}{\partial x}, \frac{1}{\mathrm{Re}}\frac{\partial v}{\partial x}, \frac{\partial P}{\partial x} + u\frac{\partial u}{\partial x} + v\frac{\partial u}{\partial y}\right)^{\mathrm{T}} \tag{8e}$$

$$F_v = \left(\frac{1}{\mathrm{Re}}\frac{\partial u}{\partial y}, \frac{1}{\mathrm{Re}}\frac{\partial v}{\partial y}, \frac{\partial P}{\partial y} + u\frac{\partial v}{\partial x} + v\frac{\partial v}{\partial y}\right)^{\mathrm{T}} \tag{8f}$$

$$H = \left(0, 0, \frac{\partial D}{\partial t}\right)^{\mathrm{T}}. \tag{8g}$$

The superscript T refers to the transpose of the vector.

Governing Equations in General Curvilinear Coordinates

In order to accommodate arbitrary geometries, the Cartesian coordinates are transformed using the following independent variables:

$$\xi = \xi(x, y)$$
$$\eta = \eta(x, y).$$

Using the general transformation by Vivian [15] and Vinokur [16], the governing equations (2), (3), and (7) are written in curvilinear coordinates, in strong conservation law form as

$$\frac{1}{J}\Gamma\frac{\partial Q}{\partial t} + \frac{\partial}{\partial \xi}[E(Q)] + \frac{\partial}{\partial \eta}[F(Q)]$$
$$= \frac{\partial}{\partial \xi}[E_{v1}(Q, Q_\xi) + E_{v2}(Q, Q_\eta)]$$
$$+ \frac{\partial}{\partial \eta}[F_{v1}(Q, Q_\xi) + F_{v2}(Q, Q_\eta)] + H, \tag{9}$$

where E and F are redefined:

$$J=\frac{\partial(\xi,\eta)}{\partial(x,y)}=\xi_x\eta_y-\xi_y\eta_x, \tag{9a}$$

$$E=\frac{1}{J}(uU+\xi_x P, vU+\xi_y P, 0)^{\mathrm{T}}, \tag{9b}$$

$$F=\frac{1}{J}(uV+\eta_x P, vV+\eta_y P, 0)^{\mathrm{T}}, \tag{9c}$$

$$E_{v1}=\frac{1}{J}\left(\frac{g^{11}}{\mathrm{Re}}\frac{\partial u}{\partial\xi}, \frac{g^{11}}{\mathrm{Re}}\frac{\partial v}{\partial\xi}, g^{11}\frac{\partial P}{\partial\xi}+U\left(\xi_x\frac{\partial u}{\partial\xi}+\xi_y\frac{\partial v}{\partial\xi}\right)\right)^{\mathrm{T}}, \tag{9d}$$

$$E_{v2}=\frac{1}{J}\left(\frac{g^{12}}{\mathrm{Re}}\frac{\partial u}{\partial\eta}, \frac{g^{12}}{\mathrm{Re}}\frac{\partial v}{\partial\eta}, g^{12}\frac{\partial P}{\partial\eta}+V\left(\xi_x\frac{\partial u}{\partial\eta}+\xi_y\frac{\partial v}{\partial\eta}\right)\right)^{\mathrm{T}}, \tag{9e}$$

$$F_{v1}=\frac{1}{J}\left(\frac{g^{12}}{\mathrm{Re}}\frac{\partial u}{\partial\xi}, \frac{g^{12}}{\mathrm{Re}}\frac{\partial v}{\partial\xi}, g^{12}\frac{\partial P}{\partial\xi}+U\left(\eta_x\frac{\partial u}{\partial\xi}+\eta_y\frac{\partial v}{\partial\xi}\right)\right)^{\mathrm{T}}, \tag{9f}$$

$$F_{v2}=\frac{1}{J}\left(\frac{g^{22}}{\mathrm{Re}}\frac{\partial u}{\partial\eta}, \frac{g^{22}}{\mathrm{Re}}\frac{\partial v}{\partial\eta}, g^{22}\frac{\partial P}{\partial\eta}+V\left(\eta_x\frac{\partial u}{\partial\eta}+\eta_y\frac{\partial v}{\partial\eta}\right)\right)^{\mathrm{T}}. \tag{9g}$$

In the above equations U and V are the contravariant components of the velocity, defined as

$$U=u\xi_x+v\xi_y \tag{10a}$$

$$V=u\eta_x+v\eta_y \tag{10b}$$

and g^{ij} $(i, j=1, 2)$ is the contravariant metric tensor defined as

$$g^{ij}=\nabla\xi_i\nabla\xi_j, \qquad \xi_1=\xi, \xi_2=\eta. \tag{10c}$$

The dilation term D in curvilinear coordinates takes the form:

$$D=\frac{\partial}{\partial\xi}\left(\frac{U}{J}\right)+\frac{\partial}{\partial\eta}\left(\frac{V}{J}\right). \tag{10d}$$

Boundary Conditions in General Curvilinear Coordinates

The Neumann boundary conditions for the pressure, Eq. (5a) and (5b), are written in general curvilinear coordinates as:

At a $\xi=$ constant boundary,

$$-\left(g^{11}\frac{\partial P}{\partial\xi}+g^{12}\frac{\partial P}{\partial\eta}\right)=U\left(\xi_x\frac{\partial u}{\partial\xi}+\xi_y\frac{\partial v}{\partial\xi}\right)+V\left(\xi_x\frac{\partial u}{\partial\eta}+\xi_y\frac{\partial v}{\partial\eta}\right)+\frac{J}{\mathrm{Re}}\frac{\partial\omega}{\partial\eta}. \tag{11a}$$

At an $\eta =$ constant boundary,

$$-\left(g^{12}\frac{\partial P}{\partial \xi}+g^{22}\frac{\partial P}{\partial \eta}\right)=U\left(\eta_x\frac{\partial u}{\partial \xi}+\eta_y\frac{\partial v}{\partial \xi}\right)+V\left(\eta_x\frac{\partial u}{\partial \eta}+\eta_y\frac{\partial v}{\partial \eta}\right)-\frac{J}{\mathrm{Re}}\frac{\partial \omega}{\partial \xi}, \tag{11b}$$

where

$$\omega = J\left[\frac{\partial}{\partial \xi}\left(\frac{v\xi_x}{J}-\frac{u\xi_y}{J}\right)+\frac{\partial}{\partial \eta}\left(\frac{v\eta_x}{J}-\frac{u\eta_y}{J}\right)\right]. \tag{11c}$$

Numerical Solutions

The implicit approximate factorization method of Beam and Warming [1] is used to solve the coupled system (9). Using Euler implicit time discretization, Eq. (8) is written at the time level $t+\Delta t=(n+1)$ as

$$\frac{1}{J}\Gamma\,\Delta Q+\Delta t\frac{\partial}{\partial \xi}(E-E_{v1}-E_{v2})^{n+1}$$

$$+\Delta t\frac{\partial}{\partial \eta}(F-F_{v1}-F_{v2})^{n+1}=\Delta t H^{n+1}, \tag{12}$$

where

$$\Delta Q = Q^{n+1}-Q^n. \tag{12a}$$

The vectors E, E_{v1}, F, F_{v2}, and H are linearized in time using Taylor's expansion, while E_{v2} and F_{v1} are evaluated explicitly in time, because they contain cross-derivative terms [1],

$$E^{n+1}(Q)=E^n(Q)+A^n\,\Delta Q \tag{12b}$$

$$E_{v1}^{n+1}(Q,Q_\xi)=E_{v1}^n(Q,Q_\xi)+R^n\,\Delta Q+S^n\frac{\partial}{\partial \xi}\Delta Q \tag{12c}$$

$$E_{v2}^{n+1}(Q,Q_\eta)=E_{v2}^n(Q,Q_\eta)+\Delta E_{v2}^{n-1} \tag{12d}$$

$$F^{n+1}(Q)=F^n(Q)+B^n\,\Delta Q \tag{12e}$$

$$F_{v1}^{n+1}(Q,Q_\xi)=F_{v1}^n(Q,Q_\xi)+\Delta F_{v1}^{n-1} \tag{12f}$$

$$F_{v2}^{n+1}(Q,Q_\eta)=F_{v2}^n(Q,Q_\eta)+M^n\,\Delta Q+N^n\frac{\partial}{\partial \eta}\Delta Q, \tag{12g}$$

where A, R, S, B, M, and N are the Jacobian matrices

$$\frac{\partial E}{\partial Q},\ \frac{\partial E_{v1}}{\partial Q},\ \frac{\partial E_{v1}}{\partial Q_\xi},\ \frac{\partial F}{\partial Q},\ \frac{\partial F_{v2}}{\partial Q},\ \frac{\partial F_{v2}}{\partial Q_\eta},$$

respectively.

The Jacobian matrices in general curvilinear coordinates are given by

$$A \text{ and } B = \frac{1}{J}\begin{bmatrix} 2k_x u + k_y v & k_y u & k_x \\ k_x v & k_x u + 2k_y v & k_y \\ 0 & 0 & 0 \end{bmatrix}, \tag{13a}$$

$$R \text{ and } M = \frac{1}{J}\begin{bmatrix} 0 & 0 & 0 \\ 0 & 0 & 0 \\ \underline{k_x\left(k_x \dfrac{\partial u}{\partial k} + k_y \dfrac{\partial v}{\partial k}\right)} & \underline{k_y\left(k_x \dfrac{\partial u}{\partial k} + k_y \dfrac{\partial v}{\partial k}\right)} & 0 \end{bmatrix}, \tag{13b}$$

$$S \text{ and } N = \frac{1}{J}\begin{bmatrix} \dfrac{1}{\mathrm{Re}}(k_x^2 + k_y^2) & 0 & 0 \\ 0 & \dfrac{1}{\mathrm{Re}}(k_x^2 + k_y^2 & 0 \\ \underline{k_x(uk_x + vk_y)} & \underline{k_y(uk_x + vk_y)} & \underline{(k_x^2 + k_y^2)} \end{bmatrix}, \tag{13c}$$

where $k = \xi$ for A, R, and S Jocabians and $k = \eta$ for B, M, and N, respectively. The underlined coefficients in (13b) and (13c) are the contribution of the pressure equation to the system of the governing equations. It can be seen from Eq. (13c) that the viscous Jacobian matrices, S and N (i.e., the coefficients of the second order spatial derivatives), have one eigenvalue which is independent of the Reynolds number. This eigenvalue results from the coupling of the pressure equation with the momentum equations. Thus, the dissipative terms in the coupled system of the governing equations (9) do not go to zero as the Reynolds number increases. This feature of the present formulation results in stable and robust computations over a wide range of Reynolds numbers. No explicit artificial dissipation is added to the system of the governing equations for stability, although central differencing is used for the spatial discretization of the convective terms.

The term $\partial D/\partial t$ in the right-hand side of Eq. (9) is approximated in time with the same order of accuracy as Q,

$$\frac{\partial D}{\partial t} = \frac{D^{n+1} - D^n}{\Delta t}. \tag{14}$$

In order to satisfy the continuity equation (1), the term D^{n+1} is set equal to zero in Eq. (14). As suggested by Harlow and Welch [7], D^n is retained in Eq. (14) in order to cure the instability arising from the differencing of the unsteady term $\partial D/\partial t$. Thus

$$\frac{\partial D}{\partial t} = -\frac{D^n}{\Delta t}. \tag{14a}$$

Using the above equations, Eq. (12) can be written as

$$\left[\Gamma + \Delta t J \frac{\partial}{\partial \xi}\left(A - R - S\frac{\partial}{\partial \xi}\right) + \Delta t J \frac{\partial}{\partial \eta}\left(B - M - N\frac{\partial}{\partial \eta}\right)\right]\Delta Q = -\Delta t J\,\mathrm{RHS}^n, \tag{15}$$

where

$$\mathrm{RHS}^n = \frac{\partial}{\partial \xi}(E - E_{v1} - E_{v2})^n + \frac{\partial}{\partial \eta}(F - F_{v1} - F_{v2})^n - H^n - \frac{\partial}{\partial \xi}(\Delta^{n-1}E_{v2}) - \frac{\partial}{\partial \eta}(\Delta^{n-1}F_{v1}) \tag{15a}$$

$$\Delta(\ )^{n-1} = (\ )^n - (\ )^{n-1}. \tag{15b}$$

Applying the approximate factorization method of Ref. [1] to Eq. (15), we obtain

$$\left[\Gamma + \Delta t J \frac{\partial}{\partial \xi}\left(A - R - S\frac{\partial}{\partial \xi}\right)\right]\Gamma^{-1}\left[\Gamma + \Delta t J \frac{\partial}{\partial \eta}\left(B - M - N\frac{\partial}{\partial \eta}\right)\right]\Delta Q = -\Delta t J\,\mathrm{RHS}^n. \tag{16}$$

Equation (16) is solved in two steps; each one involves the inversion of a block tridiagonal matrix, as follows:

$$\left[\Gamma + \Delta t J \frac{\partial}{\partial \xi}\left(A - R - S\frac{\partial}{\partial \xi}\right)\right]\Delta Q^* = -\Delta t J\,\mathrm{RHS}^n \tag{16a}$$

and

$$\left[\Gamma + \Delta t J \frac{\partial}{\partial \eta}\left(B - M - N\frac{\partial}{\partial \eta}\right)\right]\Delta Q = \Gamma\,\Delta Q^*. \tag{16b}$$

Finite-difference approximations for Eq. (16a) and (16b) are obtained using central second-order accurate formulas for both first- and second-order derivatives. With reference to Fig. 1, the first- and second-order derivatives are approximated as

$$\frac{\partial}{\partial \eta}(B\,\Delta Q) = [(B\,\Delta Q)_{i,j+1} - (B\,\Delta Q)_{i,j-1}]/2\Delta\eta \tag{17a}$$

$$\frac{\partial}{\partial \eta}\left(N\frac{\partial}{\partial \eta}\Delta Q\right) = [N_n(\Delta Q_{i,j+1} - \Delta Q_{i,j}) - N_s(\Delta Q_{i,j} - \Delta Q_{i,j-1})]/\Delta\eta^2, \tag{17b}$$

where subscripts n and s refer to grid locations $i, j+\frac{1}{2}$ and $i, j-\frac{1}{2}$, respectively.

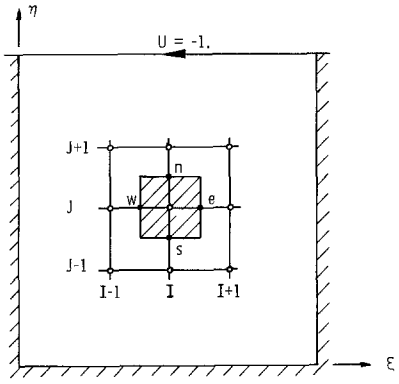

Similar expressions for the rest of the derivatives are obtained using the same method. The metric coefficients and the Jacobian of the geometric transformation are computed at the grid points (i, j) as well as the e, w, n, and s locations (Fig. 1). A simple averaging procedure is used to compute the velocity components at these locations using the computed dependent variables at the grid points (i, j).

Boundary Conditions and the Compatibility Constraint

Two levels of boundary conditions are required at the time levels (*) and $(n+1)$ because of the factorization procedure used in Eq. (16). Boundary conditions for the velocity components are obtained from the no-flux and no-slip conditions at the solid boundaries, thus $\Delta u = \Delta v = \Delta u^* = \Delta v^* = 0$.

Care must be exercised in determining the proper boundary conditions for p, Δp, and Δp^* in order to satisfy the compatibility condition of the pressure equation. Application of the Neumann boundary conditions explicitly seems to be the simplest way to implement the consistent finite-difference method of Ref. [8]. The Neumann boundary conditions are applied at one-half grid away from the boundary to compute P^n. The computed pressure is then used at the time level $n+1$. Thus, ΔP^n and ΔP^* are both set equal to zero. In other words, the Dirichlet boundary condition for the residual vector ΔQ is employed. It is important to state here that the compatibility condition must be satisfied in the right-hand side of Eq. (16a) at each time level. This is ensured by updating the pressure boundary values from the Neumann conditions.

Convergence Parameters

In this section some aspects about the stability and the convergence characteristics of system (9) are discussed. The following discussion is not a rigorous stability analysis, since this is beyond the scope of the present paper, but just an effort to estimate the parameters affecting the convergence of the coupled system.

Consider the $(t-\xi)$ plane. By locally freezing the Jacobian matrices, the following equation is obtained:

$$\frac{1}{J}\frac{\partial Q}{\partial t}+\hat{A}\frac{\partial Q}{\partial \xi}-\hat{R}\frac{\partial Q}{\partial \xi}-S\frac{\partial^2 Q}{\partial \xi^2}=\cdots. \tag{18}$$

Where $\hat{A}$, $\hat{R}$, and $\hat{S}$ are $\Gamma^{-1}A$, $\Gamma^{-1}R$, and $\Gamma^{-1}S$, respectively. The right-hand side of Eq. (18) consists of cross-derivative terms, which are evaluated explicitly in time, and η-derivative terms.

When central finite difference approximations are used to discretize the spatial derivatives the following parameters, associated with the eigenvalues of the Jacobian matrices, should be involved in the choice of the optimum time increment Δt.

$$\mathrm{CFL}=\frac{2\,|U|\,\Delta t}{\Delta \xi} \tag{19a}$$

$$\overline{\mathrm{Re}}=\frac{\Delta t g^{11}}{\mathrm{Re}\,\Delta \xi^2} \tag{19b}$$

$$\bar{\beta}=\frac{\Delta t g^{11}}{\beta\,\Delta \xi^2}. \tag{19c}$$

In order to avoid the computation of the local time steps in every iteration and save computational time, an expression involving only geometric quantities is used instead of Eq. (19a) and a CFL is defined as:

$$\mathrm{CFL}=\frac{\sqrt{g^{11}}\,\Delta t}{\Delta \xi}. \tag{19d}$$

The above expression, although it corresponds to a purely geometric variation of Δt, has been found to be adequate [17]. In the present study, CFL and $\overline{\mathrm{Re}}$ expressions are combined in one and a $\overline{\mathrm{CFL}}$ is defined as

$$\overline{\mathrm{CFL}}=\mathrm{CFL}\left(1+\frac{1}{\mathrm{Re}_{\Delta\xi}}\right), \tag{20}$$

where CFL is given by Eq. (19d) and $\mathrm{Re}_{\Delta\xi}$ is a Reynolds number based on the local grid spacing, defined by

$$\mathrm{Re}_{\Delta\xi}=\frac{\mathrm{Re}\,\Delta \xi^2}{g^{11}}. \tag{20a}$$

Given $\overline{\mathrm{CFL}}$ and $\bar{\beta}$, Eq. (20) is used to compute the local value of Δt. Then the local value of β is computed using Eq. (19c). The same analysis is applied to the $(t-\eta)$ plane by replacing $\Delta\xi$ by $\Delta\eta$ and g^{11} by g^{22}.

The parameters $\overline{CFL}$ and $\bar{\beta}$ are optimized by numerical experimentation for $Re = 100$ (see results and discussion section). The use of a variable time increment at each grid point affects the derivation of the pressure Poisson equation from the divergence of the momentum equation. The altered form of the pressure Poisson equation is given in Appendix I.

Results and Discussion

The driven cavity problem, which has been widely used for validating solution techniques for the incompressible Navier–Stokes equations, is selected to validate the present method. The method is tested at different Reynolds numbers, ranging between 100 and 1000. A stretched grid is used in order to better resolve high gradients near the solid boundaries. Furthermore, a geometric series was employed to cluster the grid near the boundaries. To preserve second-order accuracy in the physical domain the ratio of the series is chosen to be 1.1 [18].

Numerical results were obtained on several grids ranging from (11×11) to (51×51) grid points. All the results presented here are computed on (41×41) grid points for $Re = 100$ and 400 and (51×51) grid points for $Re = 1000$.

The following definition was used to compute the total residual at each time step,

$$\varepsilon_i = \sum_{j=1}^{N} |\Delta Q_{i,j}|,$$

where N is the number of grid points and $i = 1, 2, 3$ for u, v, and p residuals, respectively. The logs of the ε_i $(i = 1, 2, 3)$ are plotted versus the number of time steps.

Figure 2 present the convergence histories for u, v, and p at Reynolds numbers 100, 400, and 1000, respectively. All computations were performed without using any artificial dissipation and starting from zero initial guess. The convergence rate was optimized by numerical experimentation only for $Re = 100$. The optimum set of parameters was found to be $\overline{CFL} = 10$ and $\bar{\beta} = 60$. No effort was made to

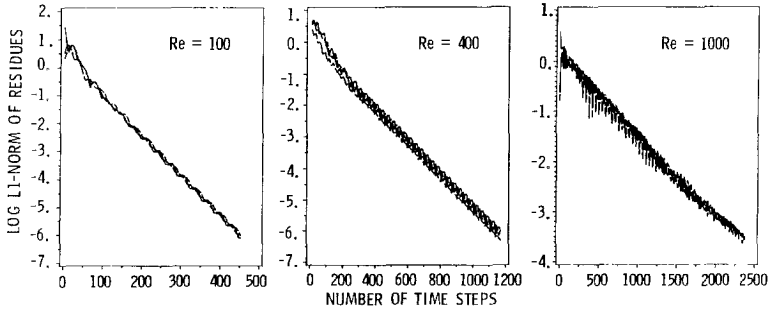

FIG. 2. Convergence histories.

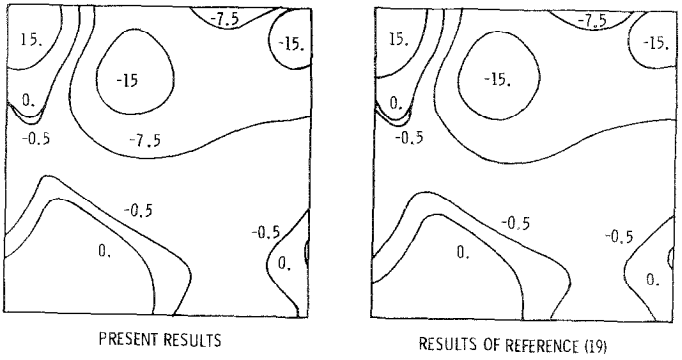

FIG. 3. Pressure coefficient contours at $Re = 100$.

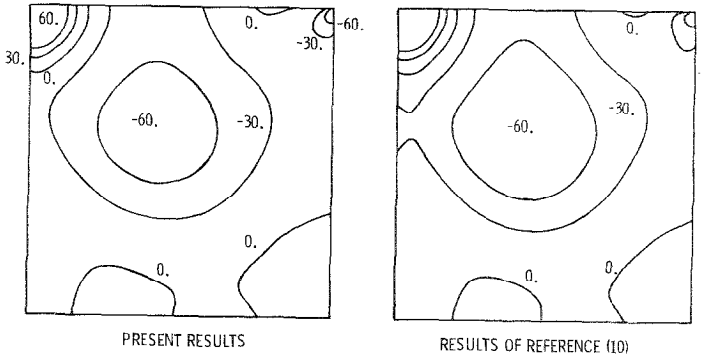

FIG. 4. Pressure coefficient contours at $Re = 400$.

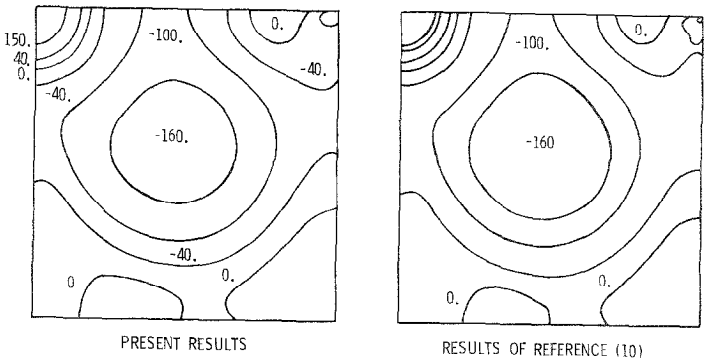

FIG. 5. Pressure coefficient contours at $Re = 1000$.

optimize the convergence at $\mathrm{Re}=400$ and 1000. For $\mathrm{Re}=400$ the same set of parameters as at $\mathrm{Re}=100$ was used. At $\mathrm{Re}=1000$ the $\overline{\mathrm{CFL}}$ was reduced to 2, because of the severe initial guess, and the same $\bar{\beta}$ was employed.

Figure 2 shows linear variations of $\log(\varepsilon_i)$ with the number of time steps and demonstrates the excellent convergence characteristics of the coupled system. It can be seen from the figures that after the impulsive start dies out, the pressure residue drops at exactly the same rate as the velocity residues, for all the three cases considered. One can also observe that the oscillations of the pressure residue increase with the Reynolds number. However, the oscillations die out after the solution passes the transient stage and thereafter the three residues decrease at the same rate.

The computed static pressure coefficients at Reynolds numbers 100, 400, and 1000, are presented in Figs. 3, 4, and 5, respectively. The static pressure coefficient is defined as

$$C_p = 2\,\mathrm{Re}(P - P_o)/U^2,$$

where P_o is the reference pressure at the center of the cavity's lower wall and U is the reference velocity. The present results are in excellent agreement with the results of Ref. [19] (for $\mathrm{Re}=100$) and Reference [10] (for $\mathrm{Re}=400$ and 1000). In Ref. [19] the pressure was computed by direct integration of the momentum equations, while in Ref. [10] the artificial compressibility method was employed. It can be seen from Fig. 4 and 5 that the artificial compressibility method predicts slightly oscillatory pressure contours near the two upper singular corners. It is stated in Ref. [10] that artificial dissipation is required by the artificial compressibility method in order to obtain reliable pressure contours even at $\mathrm{Re}=100$. However, this is not the case for the present fully implicit technique, where all the results are obtained without artificial dissipation.

The vorticity contours, which are computed from the velocity field, are shown in Figs. 6, 7, and 8 at $\mathrm{Re}=100$, 400, and 1000, respectively. The present results compare very well with the results of Ref. [19] (for $\mathrm{Re}=100$) and Ref. [20] (at

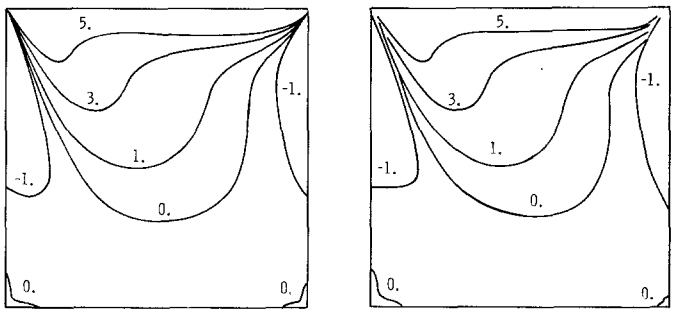

FIG. 6. Vorticity contours at $\mathrm{Re}=100$.

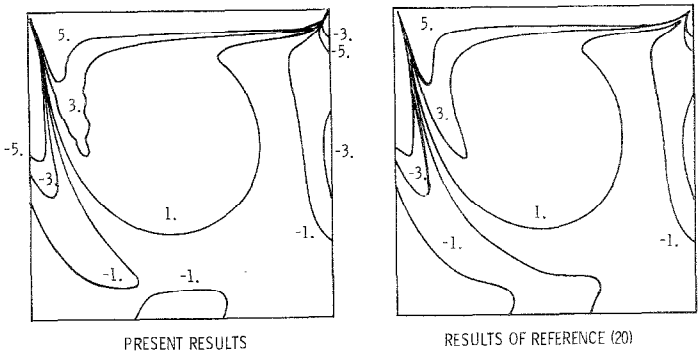

FIG. 7. Vorticity contours at $Re = 400$.

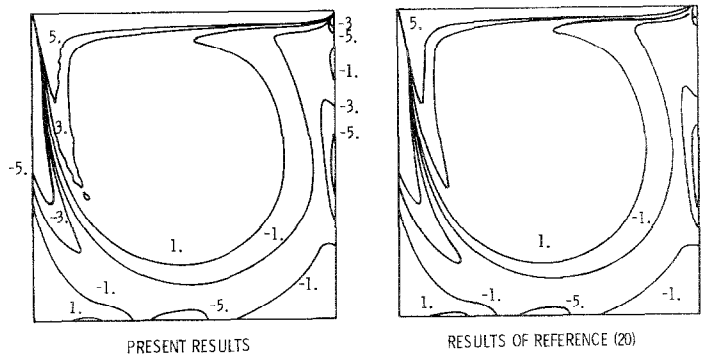

FIG. 8. Vorticity contours at $Re = 1000$.

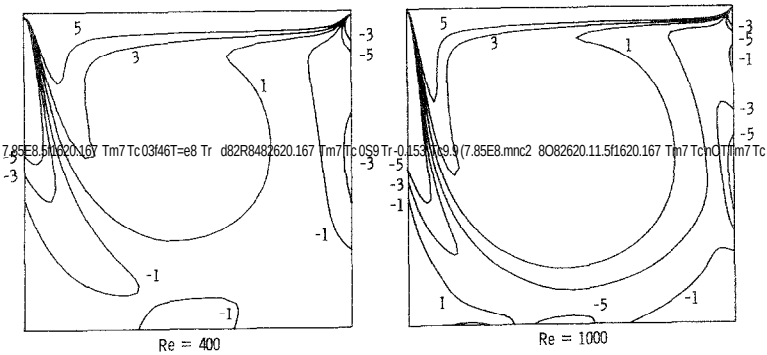

FIG. 9. Vorticity contours computed with artificial dissipation.

Re = 400 and 1000). In both references, the vorticity stream function formulation is used to solve the governing equation. The results of Ref. [19] are obtained on a (41×41) uniform grid, while in Ref. [20] the results are obtained by using a fourth-order accurate method on a (180×180) uniform grid. In the present results, one notices slight oscillatory vorticity contours in the inviscid core of the cavity, at Re = 400 and 1000. To investigate this behavior, one should examine the velocity profiles in that region, since the vorticity is not a primitive variable. Indeed there is very slight waviness in the velocity profiles in the inviscid core of the cavity. That waviness in the velocity is exaggerated in the vorticity, because the vorticity involves derivatives of the velocity field. The cause of the slight waviness is due to the odd–even decoupling which occurs locally in the inviscid core of the cavity where the viscous terms are very small and the velocity profile is amost linear.

To eliminate the waviness in the velocity field and to study the accuracy of the present method, the computations were repeated by adding fourth-order explicit artificial dissipation [18], only, to the momentum equations. The pressure equation does not require any artificial derivatives (dissipative terms). The computed vorticity contours are presented in Fig. 9 and are shown to be smooth everywhere. The velocity profiles computed with artificial dissipation are almost identical with the profiles computed without dissipation. However, the velocity profiles computed without dissipation are, indeed, slightly wavy in the inviscid core of the cavity, but this waviness can be seen only if the profiles are plotted in an exaggerated scale. This is presented in Fig. 10, where the linear part of the u-velocity profile at $x = 0.3$ is plotted in a very large scale, at Re = 400.

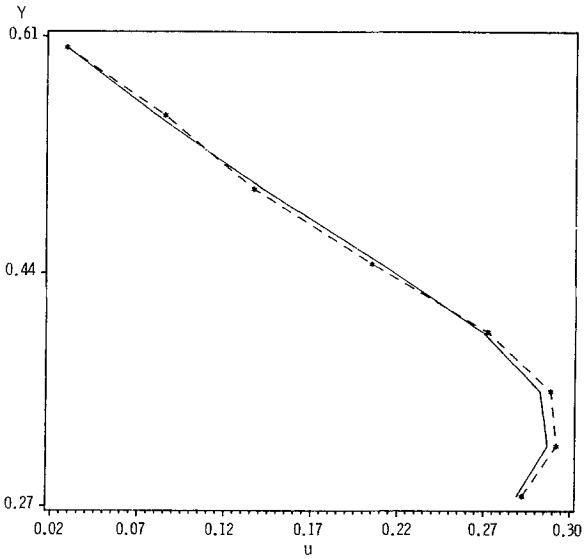

FIG. 10. Detail of the u-velocity profile at $x = 0.3$, plotted in a very large scale (Re = 400): * = results without dissipation; — = results with dissipation.

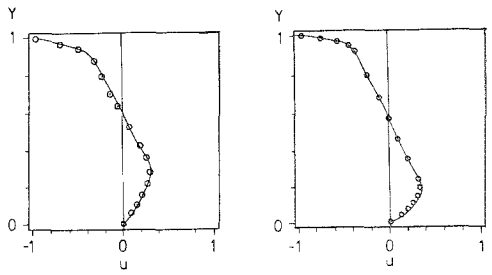

FIG. 11. u-velocity profiles at the center-line of the cavity: Re = 400; Re = 1000: — = present results; ∘ = results of Ref. [10].

The computed velocity profiles, without artificial dissipation, plotted along the vertical centerline of the cavity are in excellent agreement with the results of Ref. [10] (Fig. 11).

CONCLUSIONS

A fully implicit procedure is developed for the solution of the steady incompressible Navier–Stokes equations in primitive variables. The time dependent momentum equations are coupled with a Poisson equation for the pressure and solved using the approximate factorization method of Beam and Warming. The proposed formulation of the pressure Poisson approach does not require the iterative solution of the pressure equation at each time step. Thus, the major drawback of the classical pressure Poisson solvers is eliminated. The coupling of the pressure equation with the momentum equations results in a very stable and robust system with excellent convergence characteristics.

APPENDIX

In this Appendix, the pressure Poisson equation is derived from the momentum equations for a variable time increment. Discretizing in time the cartesian form of the momentum equations, one obtains

$$u^{n+1} = u^n - \Delta t \left(\frac{\partial P}{\partial x} + \sigma^1 + \frac{1}{\mathrm{Re}} \frac{\partial \omega}{\partial y} \right)^{n+1} \tag{I.1}$$

$$v^{n+1} = v^n - \Delta t \left(\frac{\partial P}{\partial y} + \sigma^2 - \frac{1}{\mathrm{Re}} \frac{\partial \omega}{\partial x} \right)^{n+1}, \tag{I.2}$$

where the viscous terms are expressed in terms of the vorticity and σ^1, σ^2 are the convective terms in x and y directions, respectively.

Differentiating Eq. (I.1) w.r.t. x and Eq. (I.2) w.r.t. y and adding them together, one obtains

$$\frac{\partial}{\partial x}\left[\Delta t\left(\frac{\partial P}{\partial x}+\sigma^1+\frac{1}{\mathrm{Re}}\frac{\partial \omega}{\partial y}\right)\right]^{n+1}+\frac{\partial}{\partial y}\left[\Delta t\left(\frac{\partial P}{\partial y}+\sigma^2-\frac{1}{\mathrm{Re}}\frac{\partial \omega}{\partial x}\right)\right]^{n+1}=D^n, \quad \text{(I.3)}$$

where D^{n+1} has been set equal to zero for reasons which have already been discussed.

Equation (I.3) is identical with the pressure equation (4) at steady state. This is shown by expanding Eq. (I.3) as follows:

$$\Delta t\left[\frac{\partial}{\partial x}\left(\frac{\partial P}{\partial x}+\sigma^1+\frac{1}{\mathrm{Re}}\frac{\partial \omega}{\partial y}\right)+\frac{\partial}{\partial y}\left(\frac{\partial P}{\partial y}+\sigma^2-\frac{1}{\mathrm{Re}}\frac{\partial \omega}{\partial x}\right)\right]$$
$$+\frac{\partial\,\Delta t}{\partial x}\left(\frac{\partial P}{\partial x}+\sigma^1+\frac{1}{\mathrm{Re}}\frac{\partial \omega}{\partial y}\right)+\frac{\partial\,\Delta t}{\partial y}\left(\frac{\partial P}{\partial y}+\sigma^2-\frac{1}{\mathrm{Re}}\frac{\partial \omega}{\partial x}\right)=D^n. \quad \text{(I.4)}$$

The last two brackets in Eq. (I.4) are identically zero, since they are the steady x- and y-momentum equations, respectively. Also the viscous terms can be eliminated from the remaining equation using the continuity equation and thus the pressure equation (4) is recovered. In general, curvilinear coordinates equation (I.3) is written as

$$\frac{\partial}{\partial \xi}\left[\frac{\Delta t}{J}\left(g^{11}\frac{\partial P}{\partial \xi}+g^{12}\frac{\partial P}{\partial \eta}+\sigma^1+\frac{J}{\mathrm{Re}}\frac{\partial \omega}{\partial \eta}\right)\right]$$
$$+\frac{\partial}{\partial \eta}\left[\frac{\Delta t}{J}\left(g^{12}\frac{\partial P}{\partial \xi}+g^{22}\frac{\partial P}{\partial \eta}+\sigma^2-\frac{J}{\mathrm{Re}}\frac{\partial \omega}{\partial \xi}\right)\right]=D^n, \quad \text{(I.5)}$$

where σ^1, σ^2, and D are the convective terms and the dilation in curvilinear coordinates.

The viscous terms, appearing in (I.5), are included in the cross derivative flux vectors E_{v2} and F_{v1} and, consequently, they are evaluated explicitly in time.

The Jacobian matrices of the resulting system have exactly the same form as the one given in the numerical solution section, except that the third row of the Jacobians R, N, S, and M has to be multiplied by Δt.

It is important to stress here that the Neumann boundary conditions for the pressure, given by Eq. (11a) and (11b), are absolutely consistent with Eq. (I.5). Therefore, they can be used as boundary conditions for Eq. (I.5) witnout any modifications.

Appendix: Nomenclature

A, B	Jacobian matrices $\partial E/\partial Q$ and $\partial F/\partial Q$, respectively
CFL	Courant–Friedrichs–Lewy number

C_p	Pressure coefficient
D	Dilation
E, F	ξ and η directional inviscid flux vectors, respectively
E_{v1}, F_{v1}	ξ and η directional cross viscous flux vectors, respectively
g^{ij}	Contravariant metric tensor
H	Source term
J	Jacobian of the geometric transformation
M, N	Jacobian matrices $\partial E_{v1}/\partial Q$ and $\partial F_{v2}/\partial Q$, respectively
P	Static pressure
Q	Dependent variables vector
R, S	Jacobian matrices $\partial E_{v1}/\partial Q_\xi$ and $\partial F_{v2}/\partial Q_\eta$, respectively
Re	Reynolds number
t	time
U, V	ξ and η contraviariant velocity components, respectively
u, v	x and y cartesian velocity components, respectively
x, y	Cartesian coordinates
β	Positive preconditioning parameter
Γ	Preconditioning matrix
$\Delta\xi, \Delta\eta, \Delta t$	ξ, η, and t increments, respectively
$\varepsilon_i\ (i = 1, 2, 3)$	Residual vector for u, v, and p, respectively
ξ, η	Curvilinear coordinates
σ^1, σ^2	Convection terms in ξ- and η-directions, respectively
ω	vorticity

Subscripts

e, w, n, s	Refer to east, west, north, and south of the grid point (i, j), respectively
i, j	Grid point indices
x, y	Refer to partial derivatives with respect to x and y, respectively
ξ, η	Refer to partial derivatives with respect to ξ and η, respectively
v	Refers to viscous flux vectors

Superscripts

n	Refers to time step t
T	Refers to transpose
*	Refers to time level.

Acknowledgments

This work was sponsored by the Office of Naval Research, code 12, under the direction of Dr. James Fein.

REFERENCES

1. R. BEAM AND R. F. WARMING, *AIAA J.* **16**, 393 (1978).
2. J. L. STEGER, *AIAA J.* **16**, 679 (1978).
3. A. J. CHORIN, *J. Comput. Phys.* **2**, 12 (1967).
4. J. L. STEGER AND P. KUTLER, *AIAA J.* **15**, 581 (1977).
7. F. H. Harlow and J. E. Welch, *Phys. Fluids* **8**, 2182 (1965).
8. S. ABDALLAH, *J. Comput. Phys.* **70**, 182 (1987).
9. S. ABDALLAH, *J. Comput. Phys.* **70**, 193 (1987).
10. M. L. MANSOUR AND A. HAMED, "Implicit Solutions of the Incompressible Navier–Stokes Equations in Primitive Variables," AIAA Paper 88-0717, AIAA 26th Aerospace Sciences Meeting, Reno, Nevada, Jan. 1988 (unpublished).
11. P. M. GRESHO AND R. L. SANI, *Int. J. Num. Methods Fluids* **7**, 111 (1987).
12. S. ABDALLAH AND J. DREYER, *Int. J. Num. Methods Fluids*, in press.
13. P. J. ROACHE, "Computational Fluid Dynamics" (Hermosa, Albuquerque, NM, 1976), p. 180.
14. J. H. CHEN AND S. ABDALLAH, "Computation of Incompressible Flow in Turbomachines Using the Primitive Variable Formulation," ASME Paper 87-GT, 1987 (unpublished).
15. H. VIVIAN, *Rech. Aerosp.* **1974-1**, 65 (1974).
16. M. VINOKUR, *J. Comput. Phys.* **14**, 105 (1974).
17. T. H. PULLIAM AND J. L. STEGER, "Recent Improvements in Efficiency, Accuracy and Convergence for Implicit Approximate Factorization Algorithms," AIAA Paper 85-0360, AIAA 23rd Aerospace Sciences Meeting, Reno, Nevada, Jan. 1985 (unpublished).
18. J. F. THOMPSON, Z. U. A. WARSI, AND C. M. MASTIN, *J. Comput. Phys.* **47**, 1 (1982).
19. O. R. Burggraf, *J. Fluid Mech.* **24**, 113 (1966).
20. R. SCHREIBER AND H. B. KELLER, *J. Comput. Phys.* **49**, 310 (1983).